



# Simultaneous formation of nitrogen and sulfur-doped transition metal catalysts for oxygen reduction reaction through pyrolyzing carbon-supported copper phthalocyanine tetrasulfonic acid tetrasodium salt

Xin Qing<sup>a</sup>, Jingjing Shi<sup>a</sup>, Chengyu Ma<sup>a,\*</sup>, Mengyang Fan<sup>a</sup>, Zhengyu Bai<sup>b</sup>, Zhongwei Chen<sup>c</sup>, Jinli Qiao<sup>a,b,\*</sup>, Jiujuan Zhang<sup>b,d</sup>

<sup>a</sup> College of Environmental Science and Engineering, Donghua University, 2999 Ren'min North Road, Shanghai 201620, PR China

<sup>b</sup> School of Chemistry and Chemical Engineering, Henan Normal University, Key Laboratory of Green Chemical Media and Reactions, Ministry of Education, Xinxiang 453007, PR China

<sup>c</sup> Department of Chemical Engineering, E6-2006, University of Waterloo, 200 University Avenue West, Waterloo, ON N2L 3G1, Canada

<sup>d</sup> Energy, Mining & Environment, National Research Council Canada, 4250 Wesbrook Mall, Vancouver, BC V6T 1W5, Canada

## HIGHLIGHTS

- A spontaneous formation of Cu–N–S/C catalysts was realized using a one-step pyrolysis.
- The obtained catalysts exhibit high catalytic activity for ORR in alkaline media.
- The pyrolysis process can change the ORR pathway from a 2e<sup>−</sup> transfer process to a 4e<sup>−</sup> one.
- Increasing the catalyst loading can efficiently improve the ORR activity.
- Cu-bonded graphitic–N, pyridinic–N and C–S<sub>n</sub>–C serve as the ORR catalytic sites.

## ARTICLE INFO

### Article history:

Received 17 February 2014

Received in revised form

27 April 2014

Accepted 28 April 2014

Available online 9 May 2014

### Keywords:

Doped carbon

Copper phthalocyanine

Pyrolysis effect

Active site

Oxygen reduction reaction

## ABSTRACT

In this work, we report a spontaneous formation of copper (Cu–N–S/C) catalysts containing both nitrogen (N) and sulfur (S) elements using a one-step pyrolysis of carbon supported copper phthalocyanine tetrasulfonic acid tetrasodium salt (CuTSPc/C). The obtained catalysts exhibit high catalytic activities for oxygen reduction reaction (ORR) in alkaline media. Through electrochemical measurements and physical characterizations, several observations are reached as follows: (1) different pyrolysis temperatures can result in different catalyst structures and performances, and the optimum pyrolysis temperature is found to be 700 °C; (2) the electron transfer number of the ORR process catalyzed by the unpyrolyzed catalyst is about 2.5, after the pyrolysis, this number is increased to 3.5, indicating that the pyrolysis process can change the ORR pathway from a 2-electron transfer dominated process to a 4-electron transfer dominated one; (3) increasing catalyst loading from 40 μg cm<sup>−2</sup> to 505 μg cm<sup>−2</sup> can effectively improve the catalytic ORR activity, under which the percentage of H<sub>2</sub>O<sub>2</sub> produced decreases sharply from 39.5% to 7.8%; and (4) the Cu ion can bond on pyridinic–N, graphite–N and C–S<sub>n</sub>–C to form Cu–N–S/C catalyst active sites, which play the key role in the ORR activity.

© 2014 Elsevier B.V. All rights reserved.

## 1. Introduction

With increasing energy demanding and environmental pollution, there is an urgency to explore new, efficient and sustainable energy sources to compensate and even replace traditional ones. Among different kinds of energy technologies explored, electrochemical energy technologies such as fuel cells, batteries, and supercapacitors have been considered the most feasible options. Particularly, polymer electrolyte membrane (PEM) fuel cells are

\* Corresponding authors. College of Environmental Science and Engineering, Donghua University, 2999 Ren'min North Road, Shanghai 201620, PR China. Tel.: +86 21 67792379; fax: +86 21 67792159.

E-mail addresses: [machengyu312@yahoo.com.cn](mailto:machengyu312@yahoo.com.cn) (C. Ma), [zhwchen@uwaterloo.ca](mailto:zhwchen@uwaterloo.ca) (Z. Chen), [qiaojl@dhru.edu.cn](mailto:qiaojl@dhru.edu.cn) (J. Qiao).

recognized as the most promising energy conversion devices among different electrochemical energy technologies due to their several advantages such as high energy efficiency, high energy/power densities, and low/zero emissions, as well as the wide range of applications in portable, stationary and automobile power sources [1–4]. However, there are still two major challenges hindering the commercialization of PEM fuel cells, one is high cost, and the other is insufficient durability. It has been identified that these two major challenges are closely related to the electrocatalysts used to catalyze the fuel cell cathode oxygen reduction reaction (ORR), and the anode fuel (such as hydrogen) oxidation reaction (HOR). In order to achieve high performance of PEM fuel cells, currently, the most practical electrocatalysts are Pt-based materials, which are not only expensive but also low availability. Therefore, the major effort in PEM fuel cell research and development have been put on reducing Pt loading by exploring more active catalysts, and/or replacing Pt metal using other non-precious metals such as Fe, Co and Cu.

Due to the rate of HOR is much faster than that of ORR [5–8], much more attention in PEM fuel cell development has been given to the cathode ORR catalysts rather than the anode HOR catalysts. In developing non-precious metal catalysts for PEM fuel cell ORR, several kinds of materials have been explored including transition metal macrocycles (metallic porphyrins and phthalocyanines), pyrolyzed metal-nitrogen materials, metal oxides, and chalcogenides [1–10]. Among these candidates, pyrolyzed metal–nitrogen materials supported on carbon ( $M-N_x/C$ ) seem to be the most promising ORR catalysts, especially for Fe- and/or Co-based catalysts. However, compared to Pt-based catalysts for practical application in fuel cells, this kind of non-precious metal catalysts are still facing challenges of both insufficient ORR activity and stability [2,11–14]. Although a broad range of methodologies and materials have been employed to produce active non-precious metal ORR catalysts, there are still difficulties in discerning the controlling parameters in preparing active catalysts. However, several factors have to be considered, such as type of carbon support materials, kind of transition metals, content of nitrogen in the catalyst precursor as well as the pyrolysis process, which all have effects on the catalyst's ORR activity and stability [6,10,15–17]. Among these four factors, nitrogen and carbon support are believed to be the essential components for active sites, particularly, nitrogen is approved to be the necessity for ORR activity. The metal ion in the catalytic process can be considered the necessary part of the catalytic ORR active sites ( $M-N_x/C$ ,  $x = 2$  or  $4$ ) [15,18–21] and they can also facilitate the stable incorporation of nitrogen into the graphitic structure of carbon to form other type of ORR active sites [22,23]. The pyrolysis of the corresponding materials at high temperatures, such as 600–1000 °C, is also necessary to obtain high ORR activity.

To form N-containing non-precious metal catalysts for ORR, metal phthalocyanine (MPC), which possesses a unique conjugated ligand including eight N atoms in a unit structure, and the central metal ion in the molecule, has been explored as the catalyst precursor. The pyrolyzed Co- and Fe-centered phthalocyanines have been proved to be the most promising catalysts, which were reported to have a close ORR activity to that of commercially available Pt/C catalyst [10,24–27]. In addition, it was found that different central metal ions in the MPC precursor could give different catalytic activities with an order of  $Fe > Co > Ni > Cu$  [17,20,28]. Actually, it is difficult to reveal a promotion order of the transition metals, since the ORR activity of MPC strongly depends on the pH value of electrolyte and also the composition of the catalysts as well as the preparation parameters. Recently, Sehlotho et al. [29] found that MnPc complexes could catalyze a 2-electron transfer ORR in acidic media, but 4-electron transfer one in alkaline media. Our

most recent work demonstrated that when CuPc supported on carbon black (Vulcan XC-72R) was used as the catalyst precursor, the resulting pyrolyzed CuPc/C could give an excellent ORR activity in alkaline media, and even higher than the pyrolyzed CoPc/C [30,31]. For a continuing effort, we found that if the carbon materials were doped or co-doped with other heteroatoms [32–36], such as S, P and B, the resulting catalysts could give the synergetic effect on the ORR activity. Particularly the synergetic effect between the N and S was found to be very strong, resulting in high performing ORR catalysts [37].

Inspired by the results achieved in our continuing effort, in this work, we report an ORR catalyst containing both N and S, synthesized by pyrolyzed a carbon supported CuPc precursor (copper phthalocyanine tetrasulfonic acid tetrasodium salt (CuTSPc)) which contains a both N and S in its ligand. In this way, the possible synergetic effect between N and S could be spontaneously formed within the catalyst without additional dopant precursor. As demonstrated by this work, the transition metal, nitrogen and sulfur could be simultaneously formed onto the carbon support framework to form new Cu–N–S/C catalysts. For further optimizing the catalytic activity, the effect of catalyst loading on the catalyzed ORR was also systematically investigated in this work. The electrocatalytic activities of the Cu–N–S/C catalysts obtained at different pyrolysis temperatures were intensively evaluated by linear sweep voltammetry (LSV) using both rotating disk electrode (RDE) and rotating ring-disk electrode (RRDE) techniques in alkaline media. The ORR kinetic parameters and possible reaction mechanisms were discussed. For fundamental understanding, the XRD, TEM, EDX, TG and XPS analyses were also performed to identify the possible active sites of these pyrolyzed catalysts.

## 2. Experimental

### 2.1. Materials and catalysts preparation

Copper phthalocyanine tetrasulfonic acid tetrasodium salt (CuTSPc) was purchased from Sigma Aldrich with 60% purity and used as the catalyst precursor which was supported on Vulcan XC-72R carbon black. This carbon support with a specific surface area of 236.8 m<sup>2</sup> g<sup>−1</sup> was purchased from Cabot Corporation. In preparation of such a precursor, 40 mg CuTSPc and 60 mg carbon black was mixed in a mortar, and milled by adding 10 ml methanol for 2 h, and then the resulting mixture was vacuum-dried at 40 °C for 1 h to form a powder. This powder was further placed in a quartz boat and pyrolyzed at 600 °C, 700 °C and 800 °C, respectively, for 2 h at a heating rate of 20 °C min<sup>−1</sup> in a flowing nitrogen atmosphere. The resulting catalyst powder was analyzed by instrument methods described in the section below, and expressed as (CuTSPc/C)<sub>T</sub> (here “T” means the pyrolysis temperature) For comparison, the sample of CuTSPc supported on the carbon without pyrolysis (which is the catalyst precursor) was also characterized and expressed as CuTSPc/C.

### 2.2. Catalysts characterization

The crystal-phase X-ray diffraction (XRD) patterns of both CuTSPc/C sample (or precursor) and (Cu–N–S/C)<sub>T</sub> catalyst samples were obtained using a Philips PW3830 X-ray diffractometer equipped with Cu-Kα radiation ( $\lambda = 0.15406$  nm). The measurement current was 40 mA and the voltage was 40 kV. The intensity data were collected at 25 °C in the  $2\theta$  range from 0° to 90° with a scan rate of 1.20 ° min<sup>−1</sup>. Transmission electron microscopy (TEM) analyses were performed with a high-resolution Hitachi JEM-2100F operating at 200 kV to obtain information of the average particle size and the distribution of the catalyst prepared. The element

distribution mapping was obtained by the energy dispersive X-ray spectroscopy (EDX) on JSM-5600LV (JEOL) attached to emission scanning electron microscope (SEM) on Hitachi S-4800 system, which operate at 10 kV. The thermogravimetric analysis (TGA) on a NETZSCH simultaneous thermal analyzer TG 209 can be used to analyze the mass loss during heat-treatment process. This measurement was conducted under nitrogen. The X-ray photoelectron spectroscopy (XPS) was used to study the electrocatalysts' surface or subsurface composition and detect the chemical states of their surface catalyst particles. The measurements were carried out on a Kratos AXIS Ultra<sup>DLD</sup> electron spectrometer with Al K X-ray anode source ( $h\nu = 1486.6$  eV) at 250 W and 14.0 kV. The XPSpeak 41 software was used for fitting the XPS spectrum.

### 2.3. Electrochemical measurements

The electrocatalytic activities of CuTSPc/C sample and (Cu–N–S/C)<sub>T</sub> catalysts were evaluated by linear sweep voltammetry (LSV) using both rotating disk electrode (RDE) and rotating ring-disk electrode (RRDE) techniques. A glassy carbon (GC) electrode (with a diameter of 6.0 mm corresponding to a geometric surface area of 0.25 cm<sup>2</sup>, purchased from Pine Instruments) was used as the working electrode. Before any measurements, the GC electrode surface was polished with Al<sub>2</sub>O<sub>3</sub> (0.05 μm) suspension and rinsed with deionized water. The catalyst ink was prepared by mixing 4 mg of the catalyst with 2 ml of isopropyl alcohol to form a mixture, which was then ultrasonically dispersed for 45 min to dissolve as evenly as possible. Then 10 μl of such an ink was deposited onto the GC electrode surface to form a uniform layer across the electrode surface. After drying in room temperature, one drop of methanol/Nafion<sup>®</sup> solution (50:1 wt%) was dropped onto the top of the catalyst layer to improve adhesion. For investigating the catalyst loading effect on the catalytic activity, 2, 4, 10, 25 and 40 mg of the catalyst were dispersed in 2 ml isopropyl alcohol, respectively, to form different loading of catalyst inks ( $4.0 \times 10^1$ ,  $8.0 \times 10^1$ ,  $2.0 \times 10^2$ ,  $5.0 \times 10^2$  and  $8.0 \times 10^2$  μg cm<sup>-2</sup>, respectively).

RDE measurements were carried out using a standard three-compartment electrochemical cell in 0.1 M KOH at room temperature. The GC electrode coated with catalyst was used as the working electrode. A saturated calomel electrode (SCE) was used as the reference electrode, and a platinum wire was used as the counter electrode. All measured potentials were converted to a standard hydrogen electrode (SHE). The cyclic voltammograms were performed by scanning the potential from –0.55 to 0.35 V at a scan rate of 0.05 V s<sup>-1</sup> to measure the surface behavior of the catalyst in N<sub>2</sub>-saturated 0.1 M KOH solution. For linear sweep voltammetric measurements, the used potential range was between –0.6 and 0.3 V in O<sub>2</sub>-saturated 0.1 M KOH solution. A slow scan rate of 5 mV s<sup>-1</sup> was used to record the steady-state current–potential curves. To verify the ORR catalytic pathways of the catalyst, the RRDE measurements were performed to monitor the formation of peroxide species during the ORR process.

## 3. Results and discussion

### 3.1. Oxygen reduction reaction activity

For electrochemical characterization, Fig. 1(a) shows the ORR polarization curves of Pt/C (40%) and CuTSPc/C samples synthesized before and after the pyrolysis, which were measured in O<sub>2</sub>-saturated 0.1 M KOH at room temperature. From Fig. 1(a), it can be seen that the CuTSPc/C without pyrolysis can give some ORR catalytic activity with an onset potential near –0.05 V and a half-wave potential ( $\Delta E_{1/2}$ ) near –0.17 V, respectively. However, after

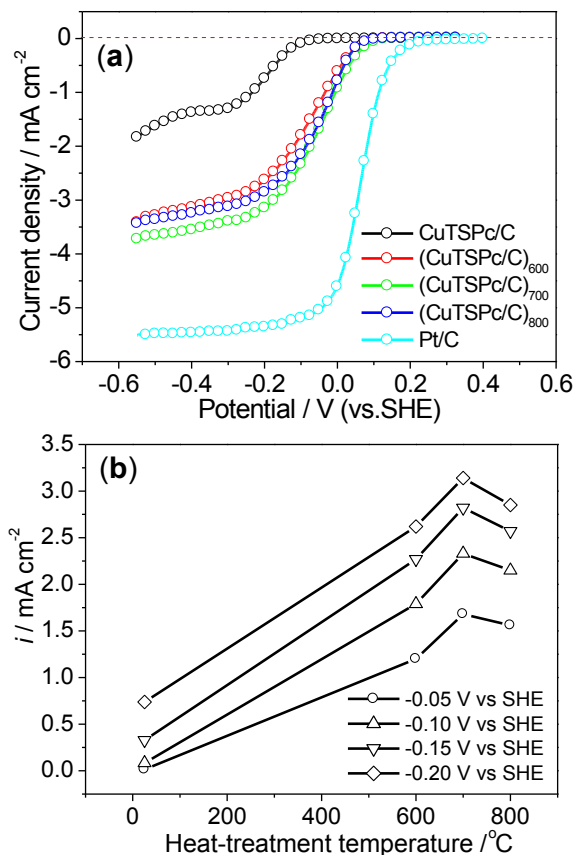


**Fig. 1.** (a) Polarization curves of ORR catalyzed by different catalysts are marked in the figure, measured in O<sub>2</sub>-saturated 0.1 M KOH solution at the ambient temperature. Scan rate: 5 mV s<sup>-1</sup>, electrode rotation rate: 1500 rpm, catalyst loading: 81 μg cm<sup>-2</sup>; (b) current densities at –0.05 V, –0.10 V, –0.15 V and –0.20 V vs. SHE as a function of catalyst pyrolysis temperature. Data from (a).

pyrolysis, the electrocatalytic activity of the catalyst is significantly improved, which is signaled by the large onset potential shifts. When the sample was pyrolyzed at 600 °C, the onset potential is shifted by a 130 mV from –0.05 V to 0.08 V, and when the sample was pyrolyzed at 700 °C, the shift is 160 mV from –0.05 V to 0.11 V. Correspondingly, the half-wave potential can be observed to positively shifted from –0.17 V (CuTSPc/C) to –0.06 V ((Cu–N–S/C)<sub>600</sub>) and further to –0.02 V ((Cu–N–S/C)<sub>700</sub>). Then, if the pyrolysis temperature is increased higher, a slight decrease in ORR activity can be observed, indicating that 700 °C may be the optimized pyrolysis temperature for synthesizing the catalysts. However, it is still lower than that for the commercial Pt-based catalyst.

To clearly show the effect of pyrolysis temperature on the ORR activity, the current densities at four potentials (–0.05 V, –0.10 V, –0.15 V and –0.20 V) as a function of temperature are plotted in Fig. 1(b). It can be seen that the current densities keep sharply increasing up to 700 °C, then starts to decrease with further increasing the pyrolysis temperature. These observations in Fig. 1 indicate that pyrolysis can significantly improve the catalyst's ORR activity. The (Cu–N–S/C)<sub>700</sub> catalyst can give the best ORR performance, probably due to the generation of the most active catalytic sites for ORR under pyrolysis temperature of 700 °C. In literature, it has been reported that pyrolysis process could largely improve the ORR activity of carbon-supported MPc catalysts, and the optimal temperature is closely dependent on the type of the central transition metal. For example, the catalytic activity of pyrolyzed CoPc/C and FePc/C catalysts could give the maximum ORR activity after pyrolysis at 600 °C [38,39], while the CuPc/C

showed the best ORR activity at 800 °C pyrolysis [31]. In this work, we found that the optimal pyrolysis temperature for CuTSPc/C was at 700 °C. Most interestingly, the ORR performance of pyrolyzed CuTSPc/C at 700 °C is even superior to either CoPc/C heat-treated at 600 °C or CuPc/C heat-treated at 800 °C [30,31], implying that the sulfur element substituted on the Pc ring (or  $-\text{SO}_3$  moiety) may make contribution to the ORR activity enhancement.

In Fig. 2, the RRDE measurements are performed to probe the ORR catalytic pathways catalyzed by the  $(\text{CuTSPc/C})_T$  catalysts obtained at different pyrolysis temperatures. The results obtained using different  $(\text{CuTSPc/C})_T$  catalysts are shown in Fig. 2(a) and (b). Based on the measurements in Fig. 2(a) and (b), the numbers of electron transferred ( $n$ ) and the percentage of peroxide species ( $\text{H}_2\text{O}_2$ ) produced can be calculated based on the formulas [40]:

$$n = \frac{4I_d}{I_d + I_r/N} \quad (1)$$

$$\%\text{H}_2\text{O}_2 = 100 \times \frac{2I_r/N}{I_d + I_r/N} \quad (2)$$

where  $I_d$ ,  $I_r$  and  $N$  are the disk current, ring current, and collection efficiency (0.37 in the present work), respectively. Based on these equations, the calculated  $\text{H}_2\text{O}_2$  percentage and the number of electron transferred, are plotted as a function of electrode potential, as shown in Fig. 2(c) and (d). It can be seen that the unpyrolyzed CuTSPc/C sample could only catalyze the ORR with a 2-electron transfer dominated process ( $n = 2.3\text{--}2.6$ ) with high  $\text{H}_2\text{O}_2$  production in the range of 68.6%–87.2% over the potential range of  $-0.10$  to  $-0.60$  V. However, all  $(\text{CuTSPc/C})_T$  catalysts can catalyze 4-electron dominated ORR processes ( $n = 3.4\text{--}3.6$ ), giving much less  $\text{H}_2\text{O}_2$  yields (around 30%). In PEM fuel cell operation, the favorite ORR process is the 4-electron transfer process from  $\text{O}_2$  to  $\text{H}_2\text{O}$  rather

than to  $\text{H}_2\text{O}_2$ . Therefore, the results in Fig. 2 indicate that the pyrolysis process could give better catalysts for fuel cell application. Due to  $(\text{CuTSPc/C})_{700}$  catalyst is the best among these samples. The  $(\text{CuTSPc/C})_{700}$  catalyst will be selected as the target catalyst for further investigation, by which we will try to find the mechanism of promotion through pyrolysis process.

For non-precious metal catalysts, the low cost is the largest advantage compared to Pt. Therefore, increasing the catalyst loading without adding significant cost could be a way to further improve the catalytic performance [31,41,42]. Fig. 3 presents RDE current–potential curves for the ORR on GC electrodes coated with different loadings of  $(\text{CuTSPc/C})_{700}$  catalyst from  $40 \mu\text{g cm}^{-2}$  to  $808 \mu\text{g cm}^{-2}$  and Pt/C (40%) at 1500 rpm, measured in  $\text{O}_2$ -saturated 0.1 M KOH. The current data in this figure is corrected by linear scanning in  $\text{N}_2$ -saturated 0.1 M KOH. Note that due to the catalyst obtained by pyrolyzed CuTSPc/C precursor at 700 °C is the most active one among those obtained at other temperatures, this  $(\text{CuTSPc/C})_{700}$  catalyst was selected as the target catalyst for investigation of the loading effect. As shown in Fig. 3, both the ORR current density (more than 200% increase) and the half-wave potential (80 mV positive shift) are largely improved with increasing catalyst loading from  $40 \mu\text{g cm}^{-2}$  to  $505 \mu\text{g cm}^{-2}$ . In addition, the ORR activity of the  $(\text{CuTSPc/C})_{700}$  catalyst with the loading at  $505 \mu\text{g cm}^{-2}$  is pretty close to that of Pt/C. When the loading is further increased to  $808 \mu\text{g cm}^{-2}$ , the current density remains the same, but the half-wave potential retreats. From what has been discussed above, it can be inferred that the optimal loading for the ORR catalyzed by  $(\text{CuTSPc/C})_{700}$  catalyst is around  $505 \mu\text{g cm}^{-2}$ . Furthermore, from Fig. 3 it can also be seen that all polarization curves can be divided into three separate potential regions. For example, the curve with catalyst loading of  $505 \mu\text{g cm}^{-2}$ , three regions are the diffusion-controlled region located in the potential range of negative than  $-0.20$  V, the Tafel region in the range of positive than  $-0.05$  V, and the mixed diffusion-kinetic limited

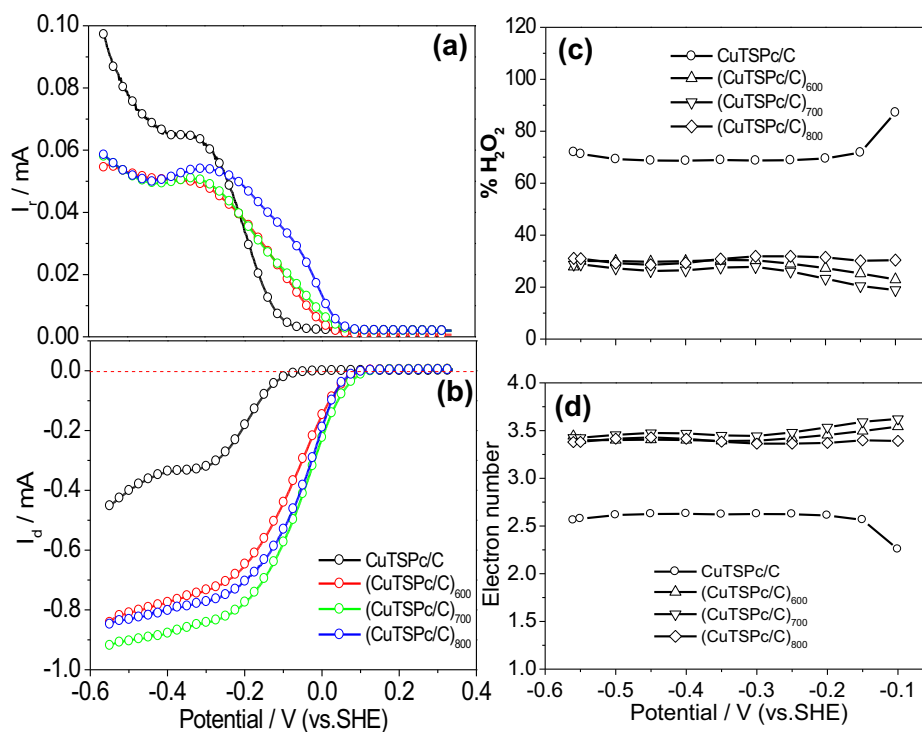


**Fig. 2.** (a) Rotating ring-disk electrode measurements for ORR catalyzed by CuTSPc/C catalysts synthesized before and after pyrolysis at a scan rate of  $5 \text{ mV s}^{-1}$  in  $\text{O}_2$ -saturated 0.1 M KOH solution; (b) the same as Fig. 1(a); (c) the corresponding  $\text{H}_2\text{O}_2$  yield; and (d) electron transfer numbers of ORR catalyzed by the sample indicated. Catalyst loading:  $81 \mu\text{g cm}^{-2}$ ; Rotating rate: 1500 rpm.

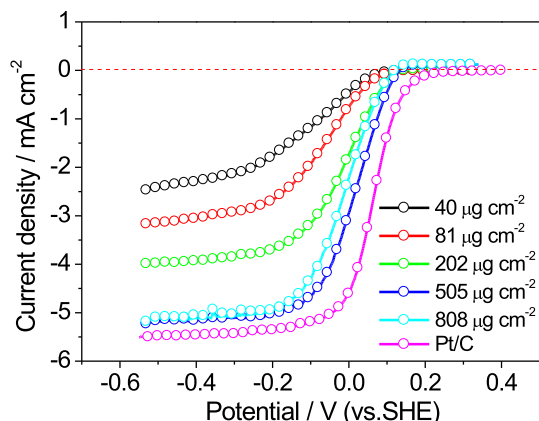


**Fig. 3.** Polarization curves of ORR catalyzed by (CuTSPc/C)<sub>700</sub> catalysts and Pt/C in O<sub>2</sub>-saturated 0.1 M KOH solution at the ambient temperature. Scan rate: 5 mV s<sup>-1</sup>, electrode rotation rate: 1500 rpm, the (CuTSPc/C)<sub>700</sub> catalysts loading: 40 μg cm<sup>-2</sup>–808 μg cm<sup>-2</sup>, the Pt/C catalyst loading: 81 μg cm<sup>-2</sup>.

region located between -0.20 V and -0.05 V, respectively. For a further comparison of the catalytic ORR activity of (CuTSPc/C)<sub>700</sub> catalyst at different loadings, the Tafel plots were constructed. The Tafel plot for cathode reaction can be expressed as Equation (3):

$$E = a - b \log \left( \frac{i_D}{i_D - i} \right) \quad (3)$$

where  $a$  is the Tafel intercept, which is related to the electrode potential at standard conditions and the ORR exchange current density,  $i$  is the diffusion-limited current density,  $i_D$  is the disk current density,  $E$  is the electrode potential, respectively.  $b$  in Equation (3), called the Tafel slope, can be expressed as Equation (4):

$$b = \frac{2.303RT}{\alpha n_\alpha F} \quad (4)$$

where  $\alpha$  and  $n_\alpha$  are the electron transfer coefficients and number in the reaction rate determining step,  $R$  is the universal gas constant,  $T$  is the temperature (K), and  $F$  is the Faraday's constant, respectively. According to Equation (3), the plot of  $E$  vs.  $\log(i_D/(i_D - i))$  can give a slope ( $2.303RT/\alpha n_\alpha F$ ), from which the kinetic parameter of  $\alpha n_\alpha$  can be calculated. In general, the larger the value of  $\alpha n_\alpha$  (or the smaller the value of Tafel slope), the faster the electrochemical reaction would be. In the case shown in Fig. 3, the values of  $\alpha n_\alpha$  obtained at different catalyst loadings should be able to tell which loading is the best for the catalyzed ORR process. Fig. 4 shows the plots of  $E$  vs.  $\log(i_D/(i_D - i))$  at different catalyst loadings. Note that the data for these Tafel plots in Fig. 4 are taken from Fig. 3. It can be seen that all Tafel plots have approximately two slopes. The values of first slope at the more positive potential range are 96, 93, 87, 78, and 81 mV dec<sup>-1</sup>, and the values of second slope are 213, 170, 159, 127, 130 mV dec<sup>-1</sup> at the catalyst loadings of 40, 81, 202, 505, and 808 μg cm<sup>-2</sup>, respectively (see Table 1). According to Equation (4), the values of kinetic parameter  $\alpha n_\alpha$  can be calculated, as listed in Table 1.

Table 1 shows that the catalyst loading of 505 μg cm<sup>-2</sup> gives the largest values of  $\alpha n_\alpha$  at both Tafel slope potential ranges, indicating that this catalyst loading is the optimum one for the catalyzed ORR by (CuTSPc/C)<sub>700</sub> catalyst. The difference in  $\alpha n_\alpha$  values at different catalyst loadings may suggest a difference in the ORR pathway catalyzed by this (CuTSPc)<sub>700</sub> catalyst, indicating that the ORR pathway can not only be affected by the type of catalyst materials [43], but also by the catalyst loading [43,44].

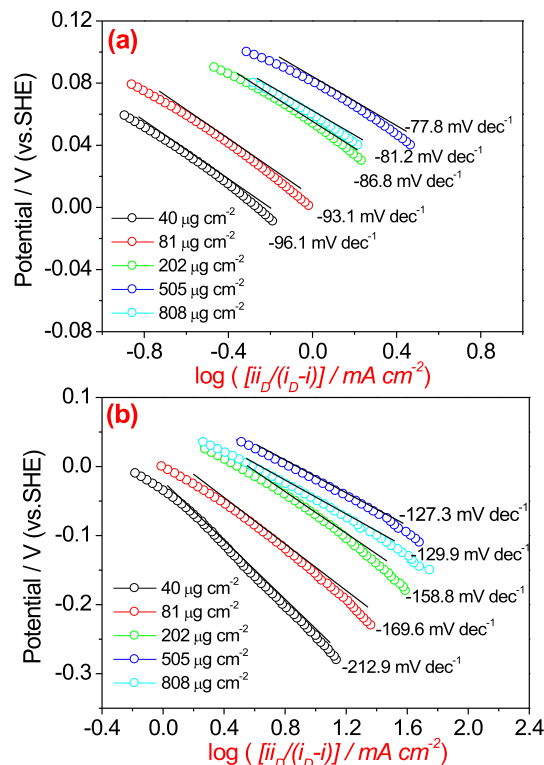


**Fig. 4.** Tafel plots of  $E$  vs.  $\log(i_D/(i_D - i))$  for ORR catalyzed by (CuTSPc/C)<sub>700</sub> catalyst at different catalyst loadings. (a) Tafel plots at high potentials and (b) Tafel plots at low potentials. Potential scan rate: 5 mV s<sup>-1</sup>, electrode rotating rate: 1500 rpm, catalyst loading: 40 μg cm<sup>-2</sup>–808 μg cm<sup>-2</sup>.

For a more quantitative evaluation, the effects of catalyst loading on the yield of H<sub>2</sub>O<sub>2</sub> and the ORR overall electron transfer number were also investigated by RRDE technique and the results are shown in Fig. 5. It can be seen that with increasing catalyst loading, the H<sub>2</sub>O<sub>2</sub> produced is sharply decreased from 39.5% at 40 μg cm<sup>-2</sup> to 7.8% at 505 μg cm<sup>-2</sup> at the potential of -0.35 V. In other words, the detection of H<sub>2</sub>O<sub>2</sub> can be effectively decreased by increasing the catalyst loading, resulting in a peroxide yield that is close to the goal established by the DOE (~3%). For the overall electron number, its value is increased accordingly from 3.2 to 3.8, suggesting that the ORR catalyzed by (CuTSPc/C)<sub>700</sub> catalyst is approached to 4e<sup>-</sup> process when the catalyst loading is increased to 505 μg cm<sup>-2</sup>. In Table 2, other kinetic parameters for ORR catalyzed (CuTSPc/C)<sub>700</sub> catalyst at different loadings, including onset potential, half-wave potential, kinetic current density, %H<sub>2</sub>O<sub>2</sub> produced and the overall electron transfer number, are summarized. From Table 2, it can be seen more intuitively that these kinetic parameters of ORR are greatly improved with increasing catalyst loading. One qualitative

**Table 1**

Product of ORR electron transfer number and coefficient in the rate-determining-step at different catalyst loadings, measured in O<sub>2</sub>-saturated 0.1 M KOH with a rotating disk electrode coated with (CuTSPc/C)<sub>700</sub> catalyst.

Catalyst loading (μg cm <sup>-2</sup> )	Tafel slope at higher potential range		Tafel slope at lower potential range	
	$b$ (mV dec <sup>-1</sup> )	$\alpha n_\alpha$	$b$ (mV dec <sup>-1</sup> )	$\alpha n_\alpha$
40	96	0.62	213	0.27
81	93	0.64	170	0.34
202	87	0.68	159	0.37
505	78	0.76	127	0.46
808	81	0.73	130	0.45

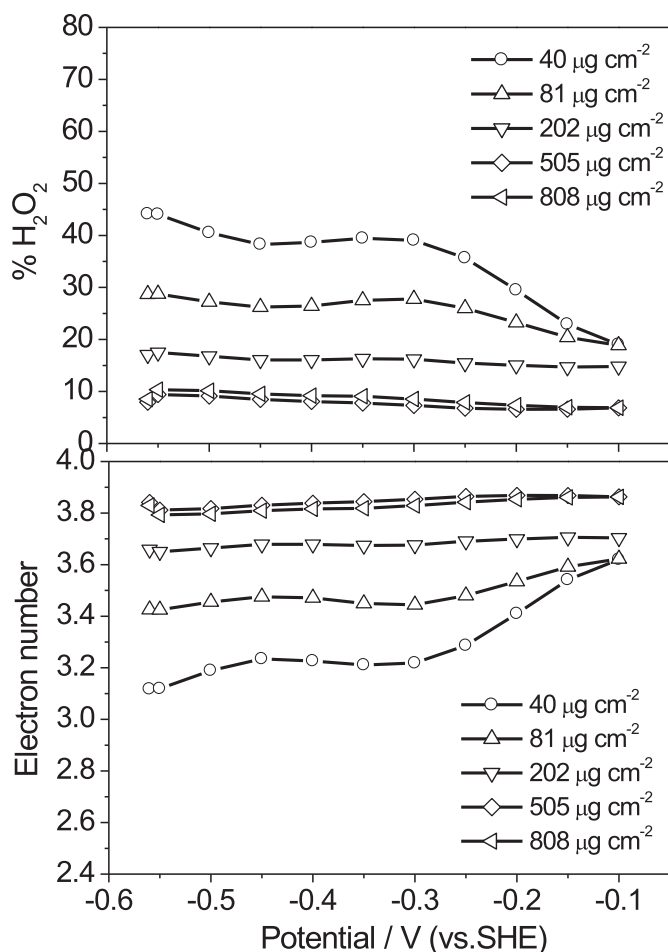


**Fig. 5.** Rotating ring-disk electrode measurements for ORR catalyzed by (CuTSPc/C)<sub>700</sub> catalysts at a scan rate of 5 mV s<sup>-1</sup> in O<sub>2</sub>-saturated 0.1 M KOH solution. (a) The corresponding %H<sub>2</sub>O<sub>2</sub> produced; and (b) electron transfer numbers of corresponding samples. Catalyst loading: 40  $\mu\text{g cm}^{-2}$ –808  $\mu\text{g cm}^{-2}$ . Rotating rate: 1500 rpm.

explanation for this loading effect could be that there are more active sites available for reducing H<sub>2</sub>O<sub>2</sub> to H<sub>2</sub>O with increasing the catalyst loading, leading to an enhanced (2 + 2) electron pathway in ORR process [45,46]. Another explanation may be considered, that is, at low loading, the catalyst layer is so thin that the generated H<sub>2</sub>O<sub>2</sub> have no enough time to stay to find neighboring active site for further reduction to water before releasing to the electrolyte, while at higher catalyst loading, H<sub>2</sub>O<sub>2</sub> have longer time to remain in catalyst layer, thus more chance for the reduction of H<sub>2</sub>O<sub>2</sub> further to water. However, too high loading will cause the catalyst layer too thick, leading to the easy cracking and falling off of the catalyst from the electrode as well as larger electric resistance, and thus resulting in lower catalytic activity.

**Table 2**  
Kinetic parameters for several loadings of (CuTSPc/C)<sub>700</sub> catalyst.

Loading ( $\mu\text{g cm}^{-2}$ )	Onset potential (V) <sup>a</sup>	$\Delta E_{1/2}$ (V) <sup>a</sup>	$j_k$ at 0.0 V (mA cm <sup>-2</sup> ) <sup>a</sup>	%H <sub>2</sub> O <sub>2</sub> at -0.35 V	$n$ at -0.35 V
40	0.10	-0.05	0.55	39.5%	3.21
81	0.11	-0.02	0.98	27.5%	3.45
202	0.13	0.00	3.06	16.3%	3.67
505	0.16	0.03	6.71	7.8%	3.84
808	0.15	0.01	3.87	9.1%	3.82

<sup>a</sup> Electrode rotation rate: 1500 rpm.

### 3.2. Morphology and structural analysis

As discussed above, the pyrolysis temperature has shown a positive effect on the ORR activity. However, the influence mechanism of pyrolysis temperature on the ORR activity is still unclear and needs to be further study. For characterizing the structure of the catalyst, XRD was employed to clarify the structure change during the pyrolysis process. XRD patterns of the CuTSPc/C precursor, (CuTSPc/C)<sub>600</sub>, (CuTSPc/C)<sub>700</sub>, and (CuTSPc/C)<sub>800</sub> catalyst samples are shown in Fig. 6. There are two large broad peaks located at  $2\theta = 24.5^\circ$  and  $2\theta = 43.0^\circ$  in all XRD patterns, which are due to the (002) and (100) reflection of carbon support (Vulcan XC-72R) [47,48]. For CuTSPc/C precursor sample, the peak at  $2\theta < 10^\circ$  can be associated with the crystalline nature of CuTSPc, which is disappeared after the pyrolysis at 600 °C, indicating that the macrocyclic structure of CuTSPc have been decomposed and then forms the Cu–N/C [38,39,49,50]. This Cu–N/C structure is considered to be the oxygen reduction active site, which may be the reason for the enhanced ORR activity of catalysts after pyrolysis. When the pyrolysis temperature is increased to 700 °C, two new peaks centered at  $2\theta = 31.9^\circ$  and  $2\theta = 34.0^\circ$  can be observed. The former peak can be assigned to sulfated copper(I)-containing compound (NaCu<sub>2</sub>(SO<sub>4</sub>)<sub>2</sub>OH·H<sub>2</sub>O) [51], the later can be assigned to be the reported Cu(OH)<sub>2</sub> [52]. These two peaks become sharpened when temperature is increased to 800 °C, suggesting a cluster aggregation at such a high temperature. In addition, all curves after pyrolysis give no conspicuous characteristic peak of metallic Cu. This implies that a large amount of Cu atoms are in the form of compounds, rather than a metal element. This may be one of the reasons that (CuTSPc/C)<sub>T</sub> catalysts exhibited much superior ORR performances compared with unpyrolyzed CuTSPc/C precursor.

To study the morphology and particle size of catalysts synthesized in this work, TEM measures were carried out. The typical TEM images, as shown in Fig. 7, can help understand the morphology and particle size differences before and after the pyrolysis. Fig. 7(a) shows a micrograph of CuTSPc/C precursor, which shows a clean surface with CuTSPc particles evenly dispersed on the carbon black with an average size of about 50 nm. After pyrolysis at 600 °C, some aggregates like Cu-containing cluster compounds appear with the particle size reduced to about 20–30 nm for large particles and about 10–20 nm for some small particles. But their shapes can not be clearly observed in Fig. 7(b). In the case of pyrolysis temperature of 700 °C (Fig. 7(c)), some bright particles with size similar to that large particles in Fig. 7(b) can be clearly observed. The illustration in Fig. 7(b) can obviously demonstrate these particles shape. Compared with CuTSPc/C precursor, there are some Cu-containing cluster compounds (may be Cu–N–S/C structure) uniformly distributed on the surface of carbon support. With further increasing the temperature to 800 °C (Fig. 7(d)), more small (with an average particle size ranging from 10 to 20 nm) particles can be observed, which may be copper hydroxide and Cu–S compound. These Cu–S compound species could also be formed by the decomposition of Cu–N–S/C species, resulting in a reduced catalytic activity of Cu–N–S/C [53]. Therefore, in order to obtain the optimal ORR activity, the pyrolysis should be not conducted at too high temperature. The results above suggest that pyrolysis can decompose the CuTSPc/C to Cu–N–S/C compounds, Cu hydroxide and Cu–S compound, which are in agreement with the conclusion from the XRD analysis in Fig. 6 and the LSV results from Fig. 1. In Fig. 1, the catalyst can reach the best ORR catalytic performance when it was pyrolyzed at 700 °C, suggesting that the most amount of active sites can be formed at this temperature. To further explain this observation, the EDX mapping images are shown in Fig. 8. Note that more highlighted light dots mean higher element concentration. From these images, it can be seen that the distribution of Cu, N

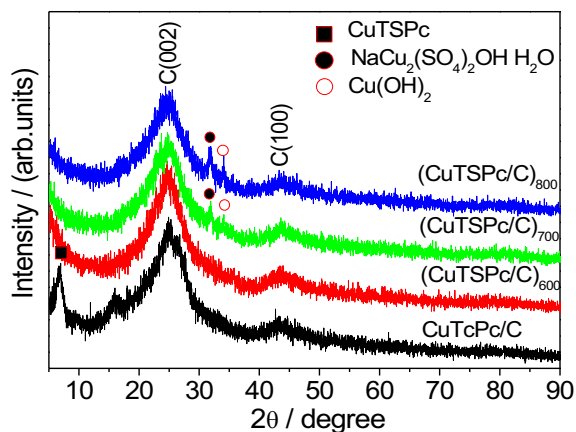


Fig. 6. X-ray diffraction spectra of the CuTSPc/C samples pyrolyzed at different temperatures.

and S become intensive after heat-treatment, especially when the temperature reaches 700 °C, suggesting that the large amount of formation of Cu–N–S structure on carbon support should be happened at 700 °C. When the temperature was further increased, the density of light dots was decreased. This can be ascribed to the damage of Cu–N–S/C structure.

### 3.3. TG analysis

Fig. 9 shows the TG–DTG curves for H<sub>2</sub>Pc/C and CuTSPc/C, respectively, to show the mass loss during the pyrolysis process. From Fig. 9(a), one can see that there is only one major peak at around 550 °C with a mass loss of about 30 wt%, is attributed to the decomposition of H<sub>2</sub>Pc [31]. In the case of the CuTSPc/C sample, the first mass loss peak at around 500 °C, which shifted to a lower

temperature by about 50 °C and the weight loss (about 8 wt%) largely decreased compared to the H<sub>2</sub>Pc/C. In addition, the peak ranging from 570 °C to 710 °C for CuTSPc/C sample is 5wt% in mass loss, which can correspond to the reengineering of catalyst structure and formation of Cu–N–S/C active structures. As shown in Fig. 1(a), the catalytic activity of CuTSPc/C after heat-treated at 700 °C is highest, therefore it can be inferred that the active sites are probably formed at about 500 °C–700 °C. The decomposition of Cu–N–S/C structures may appear at higher temperature than about 700 °C with the loss of 5 wt%, at the same time, the active sites are damaged to some extent. It is noted that the total mass loss of CuTSPc/C is smaller than that of H<sub>2</sub>Pc/C, and also smaller than that of CuPc/C [31], indicating that both Cu species and sulfonic acid group prevent phthalocyanine from thermal decomposition and contribute to higher nitrogen content which can be benefit for ORR activity sites.

### 3.4. Active site studies

For a further understanding of the catalyst activity, XPS was also employed to identify the possible active sites. Fig. 10 presents the XPS spectra of unpyrolyzed CuTSPc/C and pyrolyzed (CuTSPc/C)<sub>700</sub> samples. As shown in Fig. 10(a) and (b), five XPS peaks are observed for both unpyrolyzed and pyrolyzed samples, which correspond to the emission from S 2p, C 1s, N 1s, O 1s and Cu 2p levels. It also can be seen that the intensity of Cu 2p, O 1s, N 1s and S 2p are all decreased after the pyrolysis at 700 °C, which is given intuitively in Table 3. These decreases may not only be related to the decomposition of CuTSPc/C, but also related to encapsulation of the precursor and the pyrolysis products into the carbon matrix. We found that the results between XPS and EDX seem to be much different, which can be due to the different measurement depth and the encapsulation of the precursor and the pyrolysis products into the carbon matrix. Fig. 10(c) and (d) shows the Cu 2p spectra of unpyrolyzed and pyrolyzed samples. For CuTSPc/C precursor, the

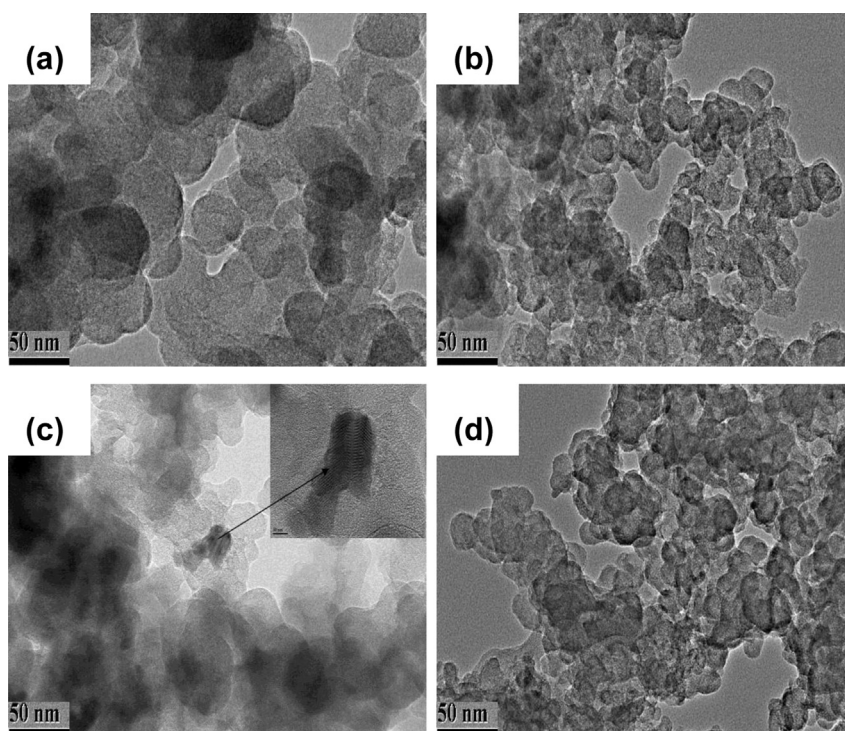


Fig. 7. TEM images of CuTSPc/C catalysts pyrolyzed at different temperatures: (a) unpyrolyzed, (b) pyrolyzed at 600 °C, (c) pyrolyzed at 700 °C and (d) pyrolyzed at 800 °C.

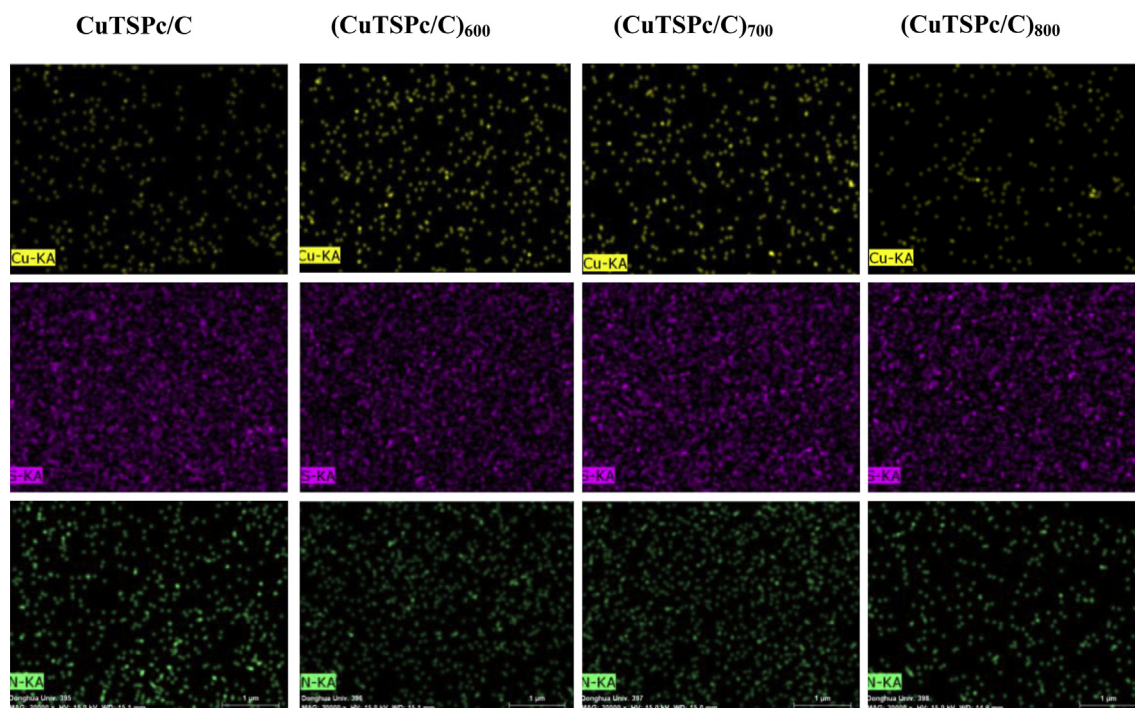


Fig. 8. EDX mapping of Cu, N and S element for CuTSPc/C catalysts without heat-treatment and heat-treated at 600 °C, 700 °C and 800 °C.

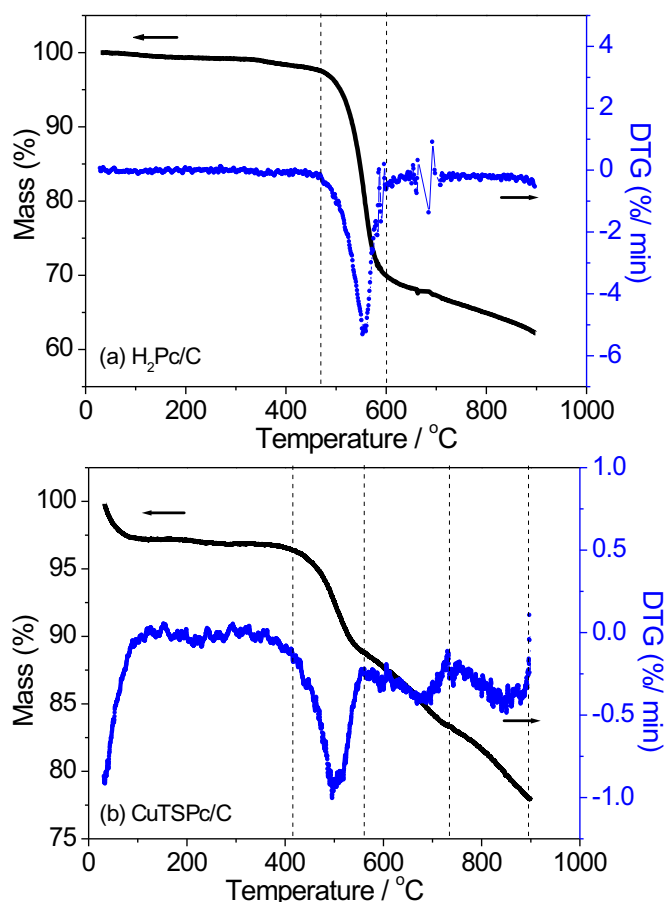
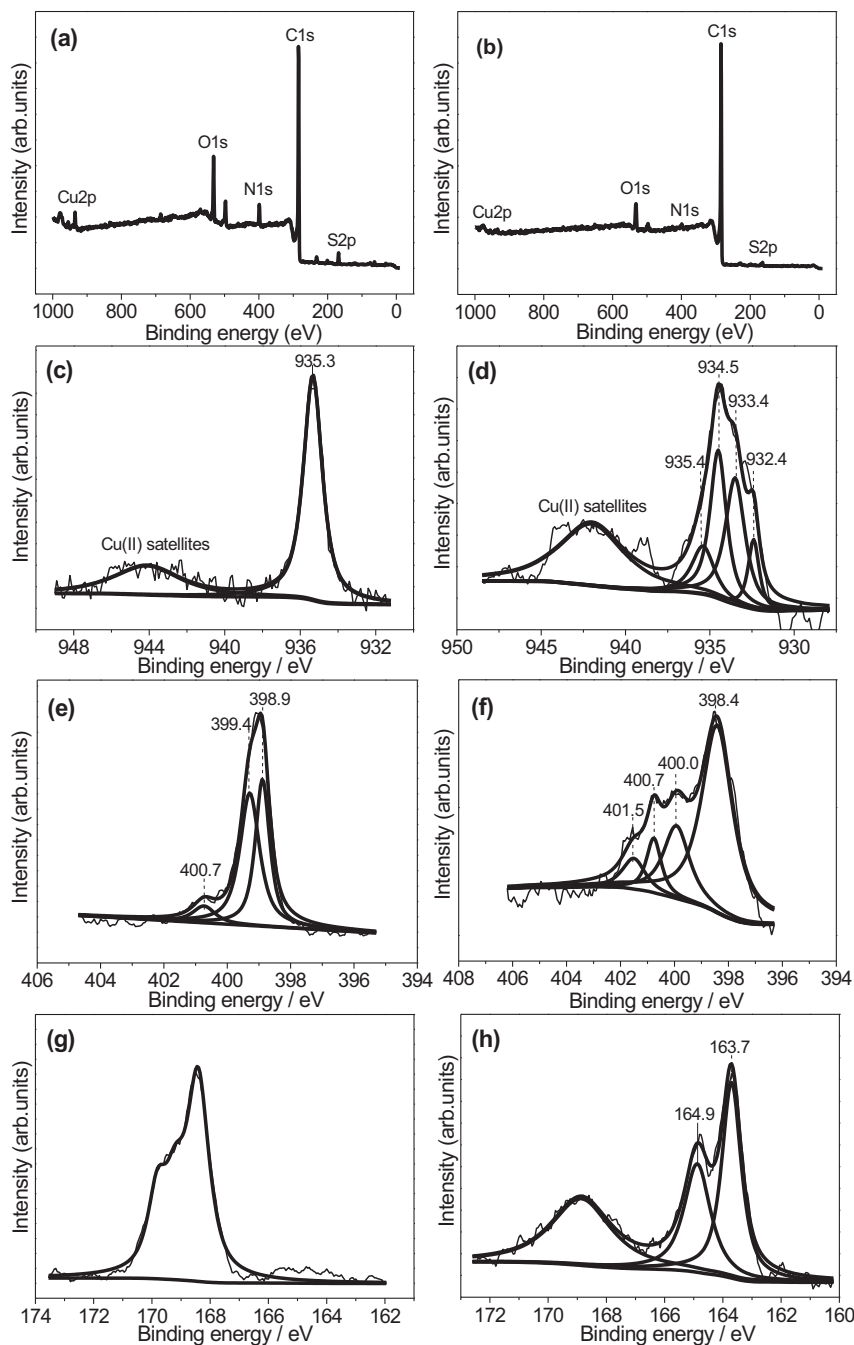


Fig. 9. TG/DTG curves for (a)  $H_2Pc/C$  and (b)  $CuTSPc/C$ .

Cu 2p spectra are characterized by the presence of a lower energy narrow main peak at 935.3 eV and a higher energy band which is originated from a broad Cu (II) satellite feature extending from 940 to 950 eV. After pyrolysis at 700 °C, the large broad peak ranging from 938 to 949 eV still stands for Cu (II) satellite. However, the Cu 2p main peak changes a lot, which can be divided into four components at 935.4, 934.5, 933.4 and 932.4 eV, respectively. The peak at 935.4 eV can be attributed to the part of undecomposed CuTSPc/C. The appearance of other three new peaks at lower banding energy are corresponding to the formation of Cu (II) hydroxide from air exposure (934.5 eV) [54,55], copper nitrides (933.4 eV) [56] and cuprous species (932.4 eV) [55,44,57].

To further determine the active species, the content of each types of Cu is shown in Fig. 11(a). It can be seen that the fitting peak area of four components for  $(CuTSPc/C)_{700}$  in Cu 2p main peak are 179.3 at 935.4 eV for Cu 2p, 402.1 at 934.5 eV for Cu (II) hydroxide, 410.6 at 933.4 eV for copper nitrides and 127.5 at 932.4 eV for cuprous species. The content of these four components above is account for 10.1%, 22.6%, 23.1% and 7.2%, respectively, indicating that the content of copper nitrides is most. Obviously, the existence of copper nitrides could be related to the formation of Cu–N–S/C active site, in other words, the generation of Cu–N–S can improve the catalytic activity of the catalyst.

Fig. 10(e) and (f) shows the N 1s binding energy region for both the unpyrolyzed and pyrolyzed samples. According to literature [58–62], the peaks of N 1s at  $398.6 \pm 0.3$  eV,  $400.5 \pm 0.3$  eV and  $401.3 \pm 0.3$  eV can be assigned to the N atoms in pyridinic ring (pyridine–N), the N atoms in pyrrolic ring (pyrrolic–N) and the N atoms as quaternary nitrogen (graphitic–N), which are generally recognized as active N species towards ORR. In the case of the unpyrolyzed CuTSPc/C sample, the N 1s band can be separated into three parts with binding energies of 398.9 eV, 399.4 eV and 400.7 eV. The peak at 399.4 eV can be assigned to amines–N [49], another two peaks can be attributed to pyridinic–N and pyrrolic–N. After pyrolyzed, two additional N 1s bands can be observed at 400.0 eV and 401.5 eV, the former energy band is assigned to C=N



**Fig. 10.** XPS spectra of (a) full-spectrum, (c) Cu 2p, (e) N 1s, (g) S 2p for unpyrolyzed CuTSPc/C; and (b) full-spectrum, (d) Cu 2p, (f) N 1s, (h) S 2p for pyrolyzed CuTSPc/C sample at 700 °C.

[58], whereas the later band is related to the graphitic–N. The other two peaks at 398.4 eV and 400.7 eV still correspond to pyridinic–N and pyrrolic–N. Although the concentration of N decreases from 4.61% (CuTSPc/C precursor) to 1.60% ((CuTSPc/C)<sub>700</sub>) as shown in Table 3, the graphitic–N forms in (CuTSPc/C)<sub>700</sub> catalyst. Moreover, the proportion of pyridinic–N strongly increases from 41.6% (CuTSPc/C precursor) to 63.1% ((CuTSPc/C)<sub>700</sub>), which can be calculated based on Fig. 11(b). What is more, both pyridinic–N and graphitic–N can combine with copper and sulfur ions to form ORR active sites (Cu–N–S/C) [62,63]. These facts could partially explain why the electrocatalytic activity of (CuTSPc/C)<sub>700</sub> is far more than that of CuTSPc/C precursor.

It was reported that sulfur-doped carbon material was a highly efficient electrocatalyst [35,36], and the pyrolysis of the catalyst in the presence of sulfur could lead to mainly amorphous carbon, resulting in increased catalyst porosity and, in turn, enhanced catalyst performance [64,65]. The results obtained for the S 2p spectral region are presented in Fig. 10(g) and (h) for unpyrolyzed and pyrolyzed samples. It can be seen that CuTSPc/C precursor without pyrolysis shows a large band ranging from 166.0 to 172.0 eV, which can be attributed to sulfite functional groups [66]. After pyrolysis at 700 °C, the region at 166.0–172.0 eV may be due to formation of sulfated copper-containing compound corresponding to the XRD of (CuTSPc/C)<sub>700</sub>. Besides, it exhibited two

**Table 3**

Concentrations (at%) of C, N, O, S and Cu in the CuTSPc/C sample and (CuTSPc/C)<sub>700</sub> catalyst, determined by XPS.

Sample	C	N	O	S	Cu
CuTSPc/C	77.45	4.61	11.47	2.07	0.91
(CuTSPc/C) <sub>700</sub>	88.71	1.60	7.05	1.27	0.38

other primary components at 163.7 eV and 164.9 eV overlapping with each other. The major contributions at binding energy around 163.7 eV can be attributed to the binding sulfurs in C–S<sub>n</sub>–C (*n* = 1 or 2) bonds, and the other band at 164.9 eV is close to that of neutral S (164.5) or the S–S bond (164.6 eV) [66,67]. Guo et al. [35] found that the –C–S–C– structure was an important factor for optimizing ORR performance. In addition, the proportion of –C–S–C– structure in the total S is about 36%, accounting for a significant proportion. This can be seen in Fig. 11(c). This fact may explain why

CuTSPc/C catalyst pyrolyzed at 700 °C shows excellent catalytic ORR activity. It should be mentioned that in the absence of sulfur, metal carbides could easily form during the decomposition process of catalyst precursor, which is no active toward ORR [6]. Our experiments in this work clearly show that there is no copper carbide detected in the heat-treated catalyst samples, suggesting that the presence of S can effectively inhibit the generation of copper carbide. In addition, the electrochemical performance of (CuTSPc/C)<sub>700</sub> is much better than our previously reported (CuPc/C)<sub>800</sub> [28]. Obviously, S is also a part of the active site in the catalyst even similar to nitrogen. Therefore, it can be concluded that both active N species and S may be the most important factors affected the ORR activity, with Cu-bonded graphitic–N, pyridinic–N and C–S<sub>n</sub>–C possibly forming the Cu–N–S/C structure and serving as the ORR catalytic sites.

#### 4. Conclusions

In conclusion, a spontaneous formation of Cu–N–S/C catalysts was successfully achieved using a one-step pyrolysis of CuTSPc compound which contains both N and S elements. The catalysts obtained at different pyrolysis temperatures are investigated toward ORR in alkaline media. Through electrochemical measurements and physical characterizations, some important results can be summarized as follows: (1) the pyrolysis temperature has significant effect on ORR activity, and the optimum pyrolysis temperature is 700 °C. Meantime, the pyrolysis process can change the ORR mechanism from a 2-electron transfer dominated process to a 4-electron transfer dominated one; (2) Increasing the catalyst loading can efficiently improve the ORR performance, and the optimal loading is around 505 μg cm<sup>−2</sup>. Under this loading, a positive shift of 60 mV for the onset potential and 80 mV for the half-wave potential are achieved compared with the loading of 40 μg cm<sup>−2</sup>. Furthermore, the detection of H<sub>2</sub>O<sub>2</sub> can be effectively decreased by increasing the catalyst loading; and (3) XRD and TEM analysis show that the ORR active sites are indeed formed after the pyrolysis. XPS results indicate that Cu ion can bond on pyridinic–N, graphitic–N, and C–S<sub>n</sub>–C to form Cu–N–S/C catalyst active sites. Therefore, both active N species and S may be the most important factors affecting the ORR activity.

#### Acknowledgment

This work was supported by the National Natural Science Foundation of China (21173039); Specialized Research Fund for the Doctoral Program of Higher Education, SRFD (20110075110001) of China; the Innovation Program of the Shanghai Municipal Education Commission (14ZZ074); Beijing Green Future Environment Foundation; Graduate Thesis Innovation Foundation of Donghua University (EG 2014015) and partially funded by Sendai-Kankyo-Kaihatsu Co. Ltd. Japan. All the financial supports are gratefully acknowledged.

#### References

- [1] C.W.B. Bezerra, L. Zhang, K. Lee, H.S. Liu, A.L.B. Marques, E. Marques, H.J. Wang, J.J. Zhang, *Electrochim. Acta* 53 (2008) 4937–4951.
- [2] Z.W. Chen, D. Higgins, A. Yu, L. Zhang, J.J. Zhang, *Energy Environ. Sci.* 4 (2011) 3167–3192.
- [3] Y.Y. Shao, J.H. Sui, G.P. Yin, Y.Z. Gao, *Appl. Catal. B: Environ.* 79 (2008) 89–99.
- [4] A. Morozan, B. Josselme, S. Palacin, *Energy Environ. Sci.* 4 (2011) 1238–1254.
- [5] A.A. Gewirth, M.S. Thorum, *Inorg. Chem.* 49 (2010) 3557–3566.
- [6] J.L. Qiao, L. Xu, L. Ding, L. Zhang, R. Baker, X.F. Dai, J.J. Zhang, *Appl. Catal. B: Environ.* 125 (2012) 197–205.
- [7] Y. Jiang, Y. Lu, X. Lv, D. Han, Q. Zhang, *ACS Catal.* 3 (2013) 1263–1271.
- [8] K. Kwon, Y.J. Sa, J.Y. Cheon, S.H. Joo, *Langmuir* 28 (2012) 991–996.
- [9] R. Jasinski, *Nature* 201 (1964) 1212–1213.

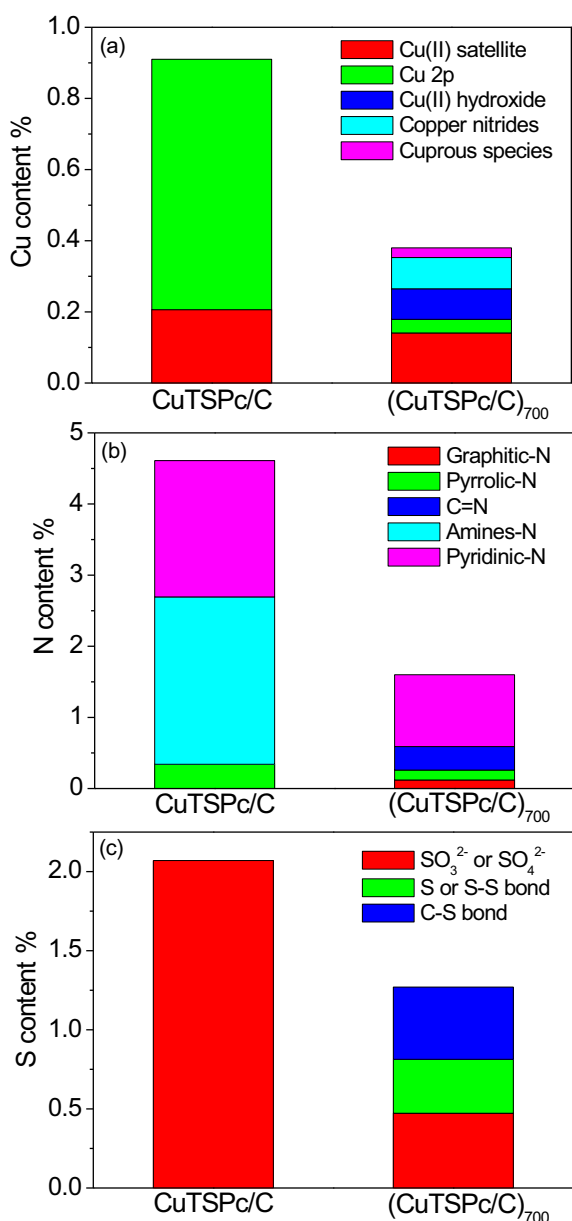


Fig. 11. The content of each types of (a) Cu; (b) N; (c) S.

- [10] I. Kruusenberg, L. Matisen, K. Tammeveski, J. Nanosci. Nanotechnol. 13 (2013) 621–627.
- [11] H. Jahnke, M. Schönbron, G. Zimmerman, Top. Curr. Chem. 61 (1976) 133–181.
- [12] H. Alt, H. Binder, G. Sandstede, J. Catal. 28 (1973) 8–19.
- [13] V.S. Bagotzky, M.R. Tarasevich, K.A. Radyushkina, O.A. Levina, J. Power Sources 2 (1978) 233–240.
- [14] X.F. Dai, J.L. Qiao, J.J. Shi, P. Xu, L. Zhang, J.J. Zhang, Int. J. Electrochem. Sci. 8 (2013) 3160–3175.
- [15] M. Lefèvre, E. Proietti, F. Jaouen, J.P. Dodelet, Science 324 (2009) 71–74.
- [16] G. Wu, K.L. More, C.M. Johnston, P. Zelenay, Science 332 (2011) 443–447.
- [17] L. Ding, X. Qing, X.J. Zhou, J.L. Qiao, H. Li, H.J. Wang, J. Appl. Electrochem. 43 (2013) 43–51.
- [18] U.I. Kossowski, I. Abs-Wurmbach, S. Fiechter, P. Bogdanoff, J. Phys. Chem. C 112 (2008) 15356–15366.
- [19] U.I. Kramm, I. Abs-Wurmbach, I. Herrmann-Geppert, J. Radnik, S. Fiechter, P. Bogdanoff, J. Electrochem. Soc. 158 (2011) B69–B78.
- [20] G. Faubert, G. Lalande, R. Côté, D. Guay, J.P. Dodelet, L.T. Weng, P. Bertrand, G. Denes, Electrochim. Acta 41 (1996) 1689–1701.
- [21] M. Lefèvre, J.P. Dodelet, P. Bertrand, J. Phys. Chem. B 106 (2002) 8705–8713.
- [22] E. Yeager, Electrochim. Acta 29 (1984) 1527–1537.
- [23] Y. Nabae, S. Moriya, K. Matsubayashi, S.M. Lyth, M. Malon, L.B. Wu, N.M. Islam, Y. Koshigoe, S. Kuroki, M.A. Kakimoto, S. Miyata, J. Ozaki, Carbon 48 (2010) 2613–2624.
- [24] R. Baker, D.P. Wilkinson, J.J. Zhang, Electrochim. Acta 53 (2008) 6906–6919.
- [25] Z.W. Xu, H.J. Li, G.X. Cao, Q.L. Zhang, K.Z. Li, X.N. Zhao, J. Mol. Catal. A: Chem. 335 (2011) 89–96.
- [26] R.R. Chen, H.X. Li, D. Chu, G.F. Wang, J. Phys. Chem. C 113 (2009) 20689–20697.
- [27] I. Kruusenberg, L. Matisen, Q. Shah, A.M. Kannan, K. Tammeveski, Int. J. Hydrogen Energy 37 (2012) 4406–4412.
- [28] Z.P. Li, B.H. Liu, J. Appl. Electrochem. 40 (2010) 475–483.
- [29] N. Sehlotho, T. Nyokong, J. Electroanal. Chem. 595 (2006) 161–167.
- [30] L. Ding, X. Qing, X.F. Dai, J. Zhang, J.L. Qiao, Ionics 19 (2013) 1415–1422.
- [31] L. Ding, J.L. Qiao, X.F. Dai, J. Zhang, J.J. Zhang, B.L. Tian, Int. J. Hydrogen Energy 37 (2012) 14103–14113.
- [32] L. Yang, S. Jiang, Y. Zhao, L. Zhu, S. Chen, X. Wang, Q. Wu, J. Ma, Y. Ma, Z. Hu, Angew. Chem. Int. Ed. 50 (2011) 7132–7135.
- [33] Z. Liu, F. Peng, H. Wang, H. Yu, J. Tan, L. Zhu, Catal. Commun. 16 (2011) 35–38.
- [34] D. Deak, E.J. Biddinger, K.A. Luthman, U.S. Ozkan, Carbon 48 (2010) 3635–3658.
- [35] H. Wang, X. Bo, Y. Zhang, L. Guo, Electrochim. Acta 108 (2013) 404–411.
- [36] R. Ahmadi, M.K. Amini, J.C. Bennett, J. Catal. 292 (2012) 81–89.
- [37] S.A. Wohlgemuth, R.J. White, M.G. Willinger, M.M. Titirici, M. Antonietti, Green Chem. 14 (2012) 1515–1523.
- [38] V. Bambagioni, C. Bianchini, J. Filippi, A. Lavacchi, W. Oberhauser, A. Marchionni, S. Moneti, F. Vizza, R. Psaro, V.D. Santo, A. Gallo, S. Recchia, L. Sordelli, J. Power Sources 196 (2011) 2519–2529.
- [39] L. Ding, X.F. Dai, R. Lin, H.J. Wang, J.L. Qiao, J. Electrochem. Soc. 159 (2012) F577–F584.
- [40] M. Lefèvre, J.P. Dodelet, Electrochim. Acta 48 (2003) 2749–2760.
- [41] G. Lalande, R. Côté, G. Tamizhmani, D. Guay, J.P. Dodelet, L. Dignard-bailey, L.T. Weng, P. Bertrand, Electrochim. Acta 40 (1995) 2635–2646.
- [42] G. Lalande, G. Tamizhmani, R. Côté, L. Dignard-bailey, M.L. Trudeau, R. Schulz, D. Guay, J.P. Dodelet, J. Electrochem. Soc. 142 (1995) 1162–1168.
- [43] J.L. Qiao, L. Xu, Y.Y. Liu, P. Xu, J.J. Shi, S.Y. Liu, B.L. Tian, Electrochim. Acta 96 (2013) 298–305.
- [44] S.L. Gojkovic, S. Gupta, R.F. Savinell, J. Electroanal. Chem. 462 (1999) 63–72.
- [45] A. Bonakdarpour, M. Lefèvre, R.Z. Yang, F. Jaouen, T. Dahn, J.P. Dodelet, J.R. Dahn, Electrochem. Solid State Lett. 11 (2008) B105–B108.
- [46] A. Velázquez-Palenzuela, L. Zhang, L.C. Wang, P.L. Cabot, E. Brillias, K. Tsay, J.J. Zhang, Electrochim. Acta 56 (2011) 4744–4752.
- [47] P. Justin, P.H.K. Charan, G.R. Rao, Appl. Catal. B: Environ. 144 (2014) 767–774.
- [48] Y.J. Hu, H. Zhang, P. Wu, H. Zhang, B. Zhou, C.X. Cai, Phys. Chem. Chem. Phys. 13 (2011) 4083–4094.
- [49] A. Velázquez-Palenzuela, L. Zhang, L.C. Wang, P.L. Cabot, E. Brillias, K. Tsay, J.J. Zhang, J. Phys. Chem. C 115 (2011) 12929–12940.
- [50] L.T. Weng, P. Bertrand, G. Lalande, D. Guay, J.P. Dodelet, Appl. Surf. Sci. 84 (1995) 9–21.
- [51] Q.Y. Liu, Z.Y. Liu, Z.P. Zhu, G.Y. Xie, Y.L. Wang, Ind. Eng. Chem. Res. 43 (2004) 4031–4037.
- [52] G.H. Du, G.V. Tendeloo, Chem. Phys. Lett. 393 (2004) 64–69.
- [53] F. Jaouen, J.P. Dodelet, Electrochim. Acta 52 (2007) 5975–5984.
- [54] W. Kautek, J.G. Gordon II, J. Electrochem. Soc. 137 (1990) 2672–2677.
- [55] T.B. Du, Y. Luo, V. Desai, Microelectron. Eng. 71 (2004) 90–97.
- [56] G. Soto, J.A. Díaz, W.D.L. Cruz, Mater. Lett. 57 (2003) 4130–4133.
- [57] S. Velu, K. Suzuki, M. Vijayaraj, S. Barman, C.S. Gopinath, Appl. Catal. B: Environ. 55 (2005) 287–299.
- [58] Q.G. He, X.F. Yang, R.H. He, A. Bueno-López, H. Miller, X.M. Ren, W.L. Yang, B.E. Koel, J. Power Sources 213 (2012) 169–179.
- [59] Y.B. Zhai, D.X. Pang, H.M. Chen, B.B. Xiang, J.J. Chen, C.T. Li, G.M. Zeng, L. Qiu, Appl. Surf. Sci. 280 (2013) 590–597.
- [60] X.G. Li, G. Liu, B.N. Popov, J. Power Sources 195 (2010) 6373–6378.
- [61] K.C. Lee, L. Zhang, H.S. Liu, R. Hui, Z. Shi, J.J. Zhang, Electrochim. Acta 54 (2009) 4704–4711.
- [62] V. Nallathambi, J.W. Lee, S.P. Kumaraguru, G. Wu, B.N. Popov, J. Power Sources 183 (2008) 34–42.
- [63] H. Niwa, K. Horiba, Y. Harada, M. Oshima, T. Ikeda, K. Terakura, J.I. Ozaki, S. Miyata, J. Power Sources 187 (2009) 93–97.
- [64] U.I. Kramm, I. Herrmann, S. Fiechter, G. Zehl, I. Zizak, I. Abs-Wurmbach, J. Radnik, I. Dorbandt, P. Bogdanoff, ECS Trans. 25 (2009) 659–670.
- [65] I. Herrmann, U.I. Kramm, J. Radnik, S. Fiechter, P. Bogdanoff, J. Electrochem. Soc. 156 (2009) 1283–1292.
- [66] H. Gao, Z. Liu, L. Song, W.H. Guo, W. Gao, L.J. Ci, A. Rao, W.J. Quan, R. Vajtai, P.M. Ajayan, Nanotechnology 23 (2012) 1–7.
- [67] J.P. Paraknowitsch, B. Wienert, Y. Zhang, A. Thomas, Chem. Eur. J. 18 (2012) 15416–15423.